Measurement of Hepatic ABCB1 and ABCG2 Transport Activity with [11C]Tariquidar and PET in Humans and Mice

Hernández Lozano, Irene ; Bauer, Martin ; Wulkersdorfer, Beatrix ; Traxl, Alexander ; Philippe, Cécile ; Weber, Maria ; Häusler, Stephanie ; Stieger, Bruno ; Jäger, Walter ; Mairinger, Severin ; Wanek, Thomas ; Hacker, Marcus ; Zeitlinger, Markus ; Langer, Oliver

Abstract: P-Glycoprotein (ABCB1) and breast cancer resistance protein (ABCG2) in the canalicular membrane of hepatocytes mediate the biliary excretion of drugs and drug metabolites. To measure hepatic ABCB1 and ABCG2 activity, we performed positron emission tomography (PET) scans with the ABCB1/ABCG2 substrate [11C]tariquidar in healthy volunteers and wild-type, Abcb1a/b(−/−), Abcg2(−/−), and Abcb1a/b(−/−)Abcg2(−/−) mice without and with coadministration of unlabeled tariquidar. PET data were analyzed with a three-compartment pharmacokinetic model. [11C]Tariquidar underwent hepatobiliary excretion in both humans and mice, and tariquidar coadministration caused a significant reduction in the rate constant for the transfer of radioactivity from the liver into bile (by −74% in humans and by −62% in wild-type mice), suggesting inhibition of canalicular efflux transporter activity. Radio-thin-layer chromatography analysis revealed that the majority of radioactivity (>87%) in the mouse liver and bile was composed of unmetabolized [11C]tariquidar. PET data in transporter knockout mice revealed that both ABCB1 and ABCG2 mediated biliary excretion of [11C]tariquidar. In vitro experiments indicated that tariquidar is not a substrate of major hepatic basolateral uptake transporters (SLCO1B1, SLCO1B3, SLCO2B1, SLC22A1, and SLC22A3). Our data suggest that [11C]tariquidar can be used to measure hepatic canalicular ABCB1/ABCG2 transport activity without a confounding effect of uptake transporters.

DOI: https://doi.org/10.1021/acs.molpharmaceut.9b01060

Measurement of hepatic ABCB1 and ABCG2 transport activity with [^{11}C]tariquidar and PET in humans and mice

Irene Hernández Lozano[1], Martin Bauer[1], Beatrix Wulkersdorfer[1], Alexander Traxl[2], Cécile Philippe[3], Maria Weber[1], Stephanie Häusler[4], Bruno Stieger[4], Walter Jäger[5], Severin Mairinger[2], Thomas Wanek[2], Marcus Hacker[3], Markus Zeitlinger[1], Oliver Langer[1,2,3,*]

[1] Department of Clinical Pharmacology, Medical University of Vienna, Vienna, Austria

[2] Preclinical Molecular Imaging, AIT Austrian Institute of Technology GmbH, Seibersdorf, Austria

[3] Division of Nuclear Medicine, Department of Biomedical Imaging and Image-guided Therapy, Medical University of Vienna, Vienna, Austria

[4] Department of Clinical Pharmacology and Toxicology, University Hospital Zurich, University of Zurich, Zurich, Switzerland.

[5] Department of Clinical Pharmacy and Diagnostics, University of Vienna, Vienna, Austria

Corresponding author:

Oliver Langer, Department of Clinical Pharmacology, Medical University of Vienna, A-1090 Vienna, Austria. Tel.: +43(0) 40400-29810, E-mail: oliver.langer@meduniwien.ac.at

Abstract

P-glycoprotein (ABCB1) and breast cancer resistance protein (ABCG2) in the canalicular membrane of hepatocytes mediate the biliary excretion of drugs and drug metabolites. To measure hepatic ABCB1 and ABCG2 activity, we performed positron emission tomography (PET) scans with the ABCB1/ABCG2 substrate [^{11}C]tariquidar in healthy volunteers and wild-type, *Abcb1a/b*$^{(-/-)}$, *Abcg2*$^{(-/-)}$ and *Abcb1a/b*$^{(-/-)}$*Abcg2*$^{(-/-)}$ mice without and with co-administration of unlabeled tariquidar. PET data were analyzed with a 3-compartment pharmacokinetic model. [^{11}C]Tariquidar underwent hepatobiliary excretion in both, humans and mice, and tariquidar co-administration caused a significant reduction in the rate constant for transfer of radioactivity from liver into bile (by -74% in humans and by -62% in wild-type mice), suggesting inhibition of canalicular efflux transporter activity. Radio-thin-layer chromatography analysis revealed that the majority of radioactivity (> 87%) in mouse liver and bile was composed of unmetabolized [^{11}C]tariquidar. PET data in transporter knockout mice revealed that both ABCB1 and ABCG2 mediated biliary excretion of [^{11}C]tariquidar. *In vitro* experiments indicated that tariquidar is not a substrate of major hepatic basolateral uptake transporters (SLCO1B1, SLCO1B3, SLCO2B1, SLC22A1 and SLC22A3). Our data suggest that [^{11}C]tariquidar can be used to measure hepatic canalicular ABCB1/ABCG2 transport activity without a confounding effect of uptake transporters.

Keywords: [^{11}C]tariquidar, ABCB1, ABCG2, liver, canalicular efflux transporter, positron emission tomography, pharmacokinetic modeling

Introduction

The liver is the major organ involved in the metabolism and excretion of drugs. Many drugs and their metabolites cannot penetrate cell membranes by passive diffusion and their hepatobiliary excretion therefore involves an interplay between uptake and efflux transporters expressed in the basolateral (sinusoidal, blood-facing) and canalicular (bile-facing) cell membranes of hepatocytes.[1, 2] Uptake of drugs from blood into hepatocytes is often mediated by basolateral transport proteins belonging to the solute carrier (SLC) family, such as organic anion-transporting polypeptides (*SLCO* family) or organic cation transporters (*SLC22A* family), while excretion from hepatocytes into bile is mainly carried out by canalicular ATP-binding cassette (ABC) transporters, such as P-glycoprotein (ABCB1), breast cancer resistance protein (ABCG2) or multidrug resistance-associated protein 2 (ABCC2).[1, 2] Accordingly, the classical well-stirred hepatic clearance model has been expanded to include drug transporters (extended clearance model).[1, 3] Alterations in hepatic transporter activities by genetic polymorphisms, drug-drug interactions (DDIs) or disease-associated mechanisms can lead to pharmacokinetic variability of transported drugs affecting their safety and efficacy.[4-6]

For an improved mechanistic understanding of the influence of transporters on hepatic drug clearance it is helpful not only to consider plasma concentrations, but also drug tissue concentrations.[7] Positron emission tomography (PET) allows for a non-invasive measurement of the tissue pharmacokinetics of radiolabeled drugs and has been applied to assess the activity of hepatic transporters,[8, 9] using radiotracers such as [^{11}C]dehydropravastatin,[10] [^{11}C]rosuvastatin,[11, 12] [^{11}C]metformin,[13] 15*R*-[^{11}C]TIC-Me,[14] [^{11}C]cholylsarcosine,[15] and [^{11}C]erlotinib.[16, 17] Although most of these radiotracers are also transported by efflux transporters in the canalicular membrane of hepatocytes, they have been primarily used to assess the activity of hepatic uptake transporters. Measuring the activity of canalicular efflux transporters is less straightforward than for uptake

transporters, as it requires knowledge of the concentrations of a probe substrate in hepatocytes and in excreted bile.

Tariquidar is a non-marketed, third-generation ABCB1 inhibitor, which has been investigated in clinical studies for its potential to overcome ABCB1-mediated multidrug resistance of tumors.[18] In microdoses as used for PET imaging, tariquidar was shown to be a substrate of murine and human ABCB1 and ABCG2, undergoing only negligible metabolism over the short duration of a PET scan.[19-21] The main route of elimination of tariquidar is hepatobiliary excretion, while urinary excretion represents only a minor route.[22, 23] PET with [^{11}C]tariquidar has been used to visualize ABCB1 and ABCG2 transport activity at the mouse and human blood-brain barrier (BBB).[19, 20, 24] We hypothesized that [^{11}C]tariquidar might be a useful probe substrate to measure the activity of ABCB1 and ABCG2 in the canalicular membrane of hepatocytes.

In this study, we performed [^{11}C]tariquidar PET imaging in healthy human volunteers and wild-type or transporter knockout mice without and with unlabeled tariquidar co-administration to assess the influence of ABCB1 and ABCG2 on the hepatobiliary excretion of [^{11}C]tariquidar.

Experimental Section

This study was conducted as a pilot study, registered with EUDRACT (number 2012-005796-14), approved by the Ethics Committee of the Medical University of Vienna, and conducted in accordance with the current version of the Declaration of Helsinki. All subjects gave their written consent before the screening examination. Study participants were defined as healthy based on medical history, physical examination, routine blood and urine laboratory testing (see Supporting Information, Table S1), and were required to be free of any medication for at least 14 days before the PET study day.

Genotyping

Venous blood samples (4 mL) were drawn from all study participants and subjects were genotyped for the *ABCG2* c.421C>A single-nucleotide polymorphism (SNP) as described previously.[19]

Radiotracer synthesis

A new batch of [^{11}C]tariquidar was synthesized for each administration and formulated in sterile 0.9% (w/v) aqueous saline solution/ethanol (9/1, v/v) containing 0.7% (v/v) polysorbate-80. For intravenous (i.v.) injection into humans an aliquot of the formulated radiotracer solution was diluted with physiological saline solution to a final volume of 10 mL.[19] Molar activity at the time of injection was 37 ± 13 GBq/μmol (n = 11 batches) and radiochemical purity was 98.7 ± 0.9%. For preclinical imaging, [^{11}C]tariquidar was formulated in a mixture of 0.9% aqueous saline/ethanol/polyethylene glycol 300 (50/15/35, v/v/v) as reported elsewhere.[20] Molar activity at the time of injection was > 100 GBq/μmol and radiochemical purity was > 98%.

Clinical PET imaging

Five male healthy volunteers (mean age: 30 ± 6 years, mean weight: 81 ± 14 kg) with unknown c.421C>A genotype at the time of enrollment and one female subject with the c.421AA genotype (60 years, 80 kg) were included into the study. Subjects underwent two consecutive dynamic 60-minute [^{11}C]tariquidar PET scans of the upper abdominal region on an Advance scanner (General Electric Medical Systems, Milwaukee, WI, USA). A first baseline scan was followed by a second scan with concurrent i.v. infusion of unlabeled tariquidar. At the start of each PET scan, a microdose of [^{11}C]tariquidar was injected as an i.v. bolus over 20 seconds (349 ± 22 MBq, corresponding to 9 ± 3 μg of unlabeled tariquidar). In parallel to PET imaging, serial blood samples were rapidly drawn every 5-7 seconds from the radial artery for the first 2.5 minutes, followed by samples taken at 3.5, 5, 10, 20, 30, 40 and 60 minutes after radiotracer injection. The second PET scan was started approximately 2 hours after the end of the baseline scan. One hour before start of the second PET scan, an i.v. infusion of unlabeled tariquidar (225 mg free base/hour, AzaTrius Pharmaceuticals, Mumbai, India) was started and maintained until the end of the second PET scan.[19] Three arterial blood samples (4 mL) were collected at the beginning, in the middle, and at the end of the second PET scan to measure plasma concentrations of tariquidar as described previously.[25] For the subject with the c.421AA genotype only the baseline PET scan was performed.

Blood and metabolite analysis

Aliquots of blood and plasma were measured for radioactivity in a gamma-counter, which was cross-calibrated with the PET camera. Selected plasma samples were analyzed for radiolabeled metabolites of [^{11}C]tariquidar using a previously described solid-phase extraction procedure.[21]

Due to the low percentage of radiolabeled metabolites in plasma, total radioactivity counts in arterial blood were considered as an input function for PET data analysis.

Preclinical PET imaging

Female wild-type (n = 5), *Abcb1a/b*$^{(-/-)}$ (n = 4), *Abcg2*$^{(-/-)}$ (n = 4), and *Abcb1a/b*$^{(-/-)}$*Abcg2*$^{(-/-)}$ (n = 5) mice with a FVB (Friend Leukemia Virus, strain B) genetic background (Taconic Inc., Germantown, NY, USA) underwent under isoflurane/oxygen anesthesia two consecutive 60-minute dynamic PET scans with [^{11}C]tariquidar (32 ± 9 MBq corresponding to < 1 µg of unlabeled tariquidar) as described previously.[20] At 2 hours before the start of the second scan, animals received an i.v. bolus injection of unlabeled tariquidar (15 mg/kg).

Assessment of radiolabeled metabolites of [^{11}C]tariquidar in mice

The study was approved by the national authorities (Amt der Niederösterreichischen Landesregierung) and study procedures were in accordance with the European Communities Council Directive of 22 September, 2010 (2010/63/EU). Female FVB mice (Charles River Laboratories, Sulzfeld, Germany) weighing 24.0 ± 0.8 g (n =4) were injected under isoflurane/oxygen anesthesia *via* the tail vein with [^{11}C]tariquidar (36 ± 4 MBq in a volume of 100 µL, formulated in 0.9% (w/v) aq. saline containing 0.1% (v/v) polysorbate-80). After a period of 30 minutes, a terminal blood sample was collected from the retro-bulbar plexus and animals were killed by cervical dislocation while under deep anesthesia. Liver, kidneys and gall bladder were removed and urine was collected. Blood was centrifuged to obtain plasma, unlabeled tariquidar (2.5 mg/mL in 2.5% glucose, 3 µL per 20 µL plasma) was added and proteins were precipitated by the addition of acetonitrile (1 µL per µL plasma). To the homogenized liver and kidney tissue, unlabeled tariquidar (2.5 mg/mL in 2.5% glucose, 3 µL per

organ) was added and proteins were precipitated by the addition of acetonitrile (800 µL for the liver, 400 µL for both kidneys). Urine and bile were precipitated by the addition of acetonitrile (1 µL per µL urine, 2 µL per µL bile). All solutions were vortexed and then centrifuged (12,000 g, 1 min, 21°C). Each supernatant (plasma, liver, bile, kidneys, urine, 5 µL each) and diluted radiotracer solution as reference were spotted on thin-layer chromatography (TLC) plates (silica gel 60F 254 nm, 10 × 20 cm; Merck, Darmstadt, Germany) and plates were developed in ethyl acetate/ethanol (6/4, v/v). Detection was performed by placing the TLC plates on multisensitive phosphor screens (Perkin-Elmer Life Sciences, Waltham, MA). The screens were scanned at 300 dpi resolution using a PerkinElmer Cyclone® Plus Phosphor Imager (Perkin-Elmer Life Sciences).

Imaging data analysis

For the clinical PET data, regions of interest for liver, combined extrahepatic bile duct and gall bladder (eBD/GB) and left renal cortex were manually delineated on individual magnetic resonance imaging (MRI) data (T1-and T2-weighted MAGNETOM Skyra 3.0T MRI, Siemens Medical Solutions, Erlangen, Germany) co-registered to PET images using PMOD 3.6 (PMOD Technologies, Zurich, Switzerland). Radioactivity in eBD/GB was assumed to represent the radioactivity excreted from liver into bile. For the mouse PET data, the left ventricle of the heart (image-derived arterial blood curve), liver, gall bladder, duodenum, intestine and left kidney were manually outlined with the medical image data examiner software AMIDE.[26] It was assumed that the sum of radioactivity in the gall bladder, duodenum and intestine represented the total radioactivity in the bile excreted from the liver. Time-activity curves (TACs) obtained from the dynamic PET data were normalized to injected dose per body weight and expressed in units of standardized uptake value (SUV = (radioactivity per g/injected radioactivity) × body weight) for

both clinical and preclinical imaging data sets. From these TACs, the area under the curve (AUC, SUV × min) was calculated using Prism 7.0 (GraphPad Software, La Jolla, CA, USA).

A previously developed 3-compartment model [27] was implemented to estimate the rate constants defining the transfer of radioactivity between blood and liver (k_1 and k_2, min^{-1}) and from liver to excreted bile (k_3, min^{-1}) (see Supporting Information, Figure S1). The radioactivity amount in the liver compartment was corrected for the amount of radioactivity in the fraction of blood in the liver.[27] This model accounts for hepatic tracer delivery *via* the portal vein and the hepatic artery (dual input function) and assumes that the measured radioactivity in tissue corresponds to unmetabolized [^{11}C]tariquidar. The radioactivity concentration in the portal vein was mathematically estimated from the measured arterial blood data and the PET data during the modeling process for both clinical and preclinical data sets.[27] The concentration in the hepatic artery corresponded to either the sampled radial artery blood for the clinical data analysis or the image-derived (from the left ventricle of the heart) arterial blood curve for the preclinical data. Hepatic uptake ($CL_{H,uptake}$) and biliary efflux ($CL_{H,bile}$) clearances were calculated as previously reported.[27] Goodness-of-fit was evaluated by visual inspection, by residual plots, by Q-Q plots and by calculating Akaike's Information Criterion, assuming a weighting function as described in detail elsewhere.[27]

In addition, a graphical analysis method called integration-plot analysis[10, 14] was used to determine the renal uptake clearance ($CL_{R,uptake}$), which defines the transfer of radioactivity from blood into the kidney. For integration plot analysis with the clinical data, the measured arterial blood radioactivity concentrations were interpolated to the midpoints of the individual PET time-frames, while the image-derived arterial blood curve was used for the preclinical data analysis. In order to obtain the total amount of radioactivity in the kidney as needed for integration plot analysis, the PET-derived radioactivity concentrations in the kidney were multiplied by reference

kidney volumes published in the literature (140 mL for humans and 0.17 mL for mice),[28] adjusted to the body weight of each individual subject.

In vitro uptake experiments

In vitro uptake experiments were performed at the Austrian Institute of Technology as described in detail elsewhere [16] with [^{11}C]tariquidar in human epidermoid carcinoma A431 cells overexpressing organic anion-transporting polypeptide 1B1, 1B3 or 2B1 (SLCO1B1, SLCO1B3, or SLCO2B1) and in A431 cells transfected with the empty vector, which had been generated as described elsewhere.[29] SLCO overexpression was confirmed by Western blotting and functionality of the SLCOs was verified by [^{3}H]estrone-3-sulfate uptake experiments. A431 cells transfected with the empty vector were used as a negative control. All cell lines were cultured in Dulbecco's modified eagle medium supplemented with 10% fetal bovine serum, 2 mM L-glutamine, 100 units/mL penicillin and 100 µg/mL streptomycin. Cells were maintained at 37°C in a humidified atmosphere of 95% air and 5% CO_2. For the uptake experiments, 5×10^5 cells per well were seeded in 24-well tissue culture plates (VWR, Radno, PA, USA) and incubated for 24 hours. On the day of the experiment, growth medium was aspirated and cells were washed with pre-warmed transport buffer (Hank's balanced salt solution supplemented with 10 mM N-2-hydroxyethylpiperazine-N-2-ethane sulfonic acid). Then the pre-warmed transport buffer was added and cells were incubated. After 30 minutes, the transport buffer was removed and pre-warmed transport buffer supplemented with 0.002% (v/v) polysorbate-80 and containing [^{11}C]tariquidar (~2 MBq per well, approximately 0.05 µM) was added and cells were incubated for additional 0.3, 2, 5, 10, 15, 20 and 30 minutes. Cell count was determined on separate 24-well tissue culture plates after each experiment. Radiotracer solutions were aspirated following incubation and cells were washed twice with ice-cold transport buffer. Cells were detached using

trypsin EDTA (0.25%) and transport buffer was added to transfer the cell suspension into tubes, which were measured for radioactivity in a gamma-counter. The uptake experiments were performed 2 times with 3 technical replicates each and radioactivity in cells was corrected for radioactive decay and expressed as percent of applied dose per 10^6 cells (%AD/1×10^6 cells).

In addition, *in vitro* uptake experiments were performed at the University Hospital Zurich with [^{3}H]tariquidar (American Radiolabeled Chemicals Inc., St. Louis, MO, USA) in wild-type human embryonic kidney cortex (HEK 293) cells or HEK 293 cells overexpressing organic cation transporter 1, 2 or 3 (SLC22A1, SLC22A2, SLC22A3) or organic cation/carnitine transporter 2 (OCTN2/SLC22A5) or organic cation/ergothioneine transporter 1 (OCTN1/SLC22A4), which were generous gifts of Drs. I Tamai and H. Koepsell. Wild-type HEK 293 cells were cultured in Dulbecco's modified Eagle's medium supplemented with 10% (v/v) fetal bovine serum, 100 units/mL penicillin and 100 µg/mL streptomycin. The characterization and cultivation of stably transfected cells was done as previously described.[30-32] Briefly, the culture medium for the SLC-transfected cell lines additionally contained Geneticin (G-418) as selecting agent (400 µg/mL for SLC22A1-, SLC22A2- and SLC22A3- and 600 µg/mL for SLC22A4- and SLC22A5-overexpressing cells). For uptake experiments with [^{3}H]tariquidar, HEK 293 cells were grown on Petri dishes coated with poly-D-lysine. 24 hours before the uptake experiment, cells were treated with 5 mM sodium butyrate. Before uptake experiments, cells were rinsed three times with 2 mL pre-warmed uptake buffer: 116.4 mM NaCl, 5.3 mM KCl, 1.0 mM NaH_2PO_4, 0.8 mM $MgSO_4$, 5.5 mM D-glucose and 20 mM HEPS/Trips pH 7.4.[33] Uptake was initiated by addition of pre-warmed uptake buffer containing labeled and unlabeled tariquidar (total concentration: 1 µM). Uptake was stopped after an incubation time of 5 minutes at 37°C by aspiration of the radiolabeled solution and rinsing the cells 4 times with 2 mL ice-cold uptake buffer. Cells were solubilized for at least 30 minutes with 1% Triton X-100 and 500 µL of this suspension were

used for radioactivity measurement by liquid scintillation counting.[34, 35] The uptake experiments were performed 2-4 times with at least 3 technical replicates each and tariquidar uptake in cells was expressed as pmol tariquidar per mg protein.

Statistical analysis

Statistical analysis was performed using Prism 7.0. After confirmation of normal distribution of the data using the Shapiro-Wilk normality test, differences in pharmacokinetic parameters between scans were assessed using a two-tailed paired t-test. Differences in parameters between mouse groups were analyzed by one-way ANOVA followed by a Tukey's multiple-comparison test. To assess correlations, the Pearson correlation coefficient (r) was calculated. The level of statistical significance was set to a p value of less than 0.05. All values are given as mean ± standard deviation (SD).

Results

Healthy volunteers underwent two consecutive PET scans with [^{11}C]tariquidar, a first baseline scan in which a microdose of tariquidar was injected (< 10 μg) and a second scan with concurrent i.v. infusion of unlabeled tariquidar (225 mg/h). Subjects were genotyped for the *ABCG2* SNP c.421C>A after the clinical part of the study. Our study cohort included four subjects with the c.421CC and one subject with the c.421CA genotype. In addition, one subject with known c.421AA genotype was included, for whom only the baseline scan was performed for safety reasons.

Adverse events occurring during study participation for which a relationship with tariquidar administration could not be excluded were dysgeusia (two subjects), vertigo (two subjects), hypotension (two subjects) and phlebitis (one subject). In each subject, tariquidar plasma concentrations were relatively constant during the second PET scan with a mean concentration across all subjects (average of three determinations at beginning, middle, and end of PET scan) of 3.0 ± 0.9 μmol/L (see Supporting Information, Figure S2a).

For the duration of both PET scans, the majority of radioactivity in plasma was composed of unmetabolized [^{11}C]tariquidar without significant differences found between the two scans (percentage of unchanged [^{11}C]tariquidar in plasma at 40 minutes after radiotracer injection, scan 1: 92.6 ± 0.9% and scan 2: 94.3± 1.9%). Serial PET images of the abdominal region (Figure 1) indicated rapid and high radioactivity uptake in the liver and excretion of radioactivity into the gall bladder at later time points of the first scan. In the second scan, radioactivity concentration in the liver and the gall bladder was reduced as compared to scan 1. The total amount of radioactivity (percentage of the injected dose) in the liver and combined extrahepatic bile duct and gall bladder (eBD/GB) at 60 min after radiotracer injection was 27.8 ± 5.3% and 0.8 ± 0.9%, respectively, in scan 1 and 26.9 ± 2.1% and 0.1 ± 0.1%, respectively, in scan 2.

In none of the subjects, emptying of the gall bladder was observed during the PET scan. In Figure 2, time-activity curves (TACs) for arterial blood, liver, and eBD/GB are shown. AUC_{blood} was significantly increased in scan 2 and AUC_{liver} was significantly decreased leading to a significant reduction in the AUC_{liver}/AUC_{blood} ratio (see Supporting Information, Table S2). We used a previously developed pharmacokinetic model (see Supporting Information, Figure S1)[27] to estimate the rate constants for transfer of radioactivity from blood into liver (k_1), from liver into blood (k_2) and from liver into excreted bile (k_3) (Table 1). The model provided good fits for both the liver and eBD/GB PET data (see Supporting Information, Figure S3). Mean parameters estimates for both scans are given in Table 1. Changes in outcome parameters between the two scans are depicted in Figure 3. k_1 values showed a significant decrease in scan 2, k_2 was not different between the two scans and k_3 was significantly decreased in the second scan. There was a trend for a correlation between the percentage change in k_3 from scan 1 to scan 2 and the mean tariquidar plasma concentrations in scan 2, but statistical significance was not reached (see Supporting Information, Figure S2b). The subject with the c.421CA genotype had the lowest k_3 reduction in scan 2 among all subjects, but this could not be explained by tariquidar plasma concentrations. Moreover, the subjects with the c.421CA and c.421AA genotypes had the lowest k_3 values in scan 1 among all subjects (Figure 3c). Hepatic uptake clearance ($CL_{H,uptake}$) was in a similar range as the human liver blood flow rate (21 mL/min/kg body weight)[28] and showed a significant reduction in scan 2 (Table 1). Hepatic biliary efflux clearance ($CL_{H,bile}$) showed a trend for a decrease in scan 2 without reaching statistical significance ($p = 0.0507$). However, if the subject with the c.421CA genotype (for whom tariquidar co-infusion caused only a small reduction in the k_3 value) was excluded from the analysis, there was a significant decrease ($p = 0.0372$) in $CL_{H,bile}$ from scan 1 (0.0231 ± 0.0130 mL/min/kg) to scan 2 (0.0041 ± 0.0037 mL/min/kg). Radioactivity concentrations in the kidneys were lower as compared to the liver and

similar in the two scans (see Supporting Information, Figure S4). Integration plot analysis was used to determine the renal uptake clearance ($CL_{R,uptake}$) which did not significantly differ between scans (0.52 ± 0.12 and 0.51 ± 0.14 mL/min/kg in scan 1 and 2, respectively) (see Supporting Information, Table S3).

Furthermore, we studied [^{11}C]tariquidar disposition in wild-type and ABC transporter knockout mice (*Abcb1a/b*$^{(-/-)}$, *Abcg2*$^{(-/-)}$, and *Abcb1a/b*$^{(-/-)}$*Abcg2*$^{(-/-)}$) without and with i.v. pre-treatment with unlabeled tariquidar. We also analyzed the percentage of unmetabolized [^{11}C]tariquidar in different tissues and fluids of wild-type mice at 30 minutes after radiotracer injection. These experiments revealed that the majority of radioactivity in plasma (78.3%), liver (92.8%) and bile (87.5%) was composed of unmetabolized [^{11}C]tariquidar (Table 2). Serial PET images showed that radioactivity was rapidly taken up by the liver (67 ± 7% of the injected dose) and distributed at later time points to the gall bladder and intestine in wild-type mice without tariquidar pre-treatment (Figure 4). In contrast, in tariquidar pre-treated wild-type mice and in *Abcb1a/b*$^{(-/-)}$*Abcg2*$^{(-/-)}$ mice radioactivity excretion into the gall bladder and intestine was considerably reduced or almost absent. The urinary bladder was not visible on the PET images in any of the studied mouse groups. The estimated amount of radioactivity excreted into the urine was very low (approximately 0.2% of the injected dose in wild-type mice at the end of the PET scan). The blood, liver, intestine and kidney TACs for all studied mouse groups are shown in Figure S5 of the Supporting Information and AUC values are given in Table S2 of the Supporting Information. Pre-treatment with tariquidar resulted in a significant increase in AUC_{blood} in wild-type mice, which was of similar magnitude as in humans. In all three knockout mouse strains, AUC_{blood} was significantly higher in scan 1 than in wild-type mice. The pharmacokinetic model was applied to the mouse PET data and provided comparably good fits as for the human data (see Supporting Information, Figure S6). k_1 and k_2 values did not differ between scans in any of the studied mouse

genotypes (Table 3 and Figure 5). Moreover, for the baselines scans, k_1 and k_2 values were not significantly different between wild-type and transporter knockout mice. Like in humans, k_3 showed a significant reduction in scan 2 in wild-type, *Abcb1a/b*$^{(-/-)}$ and *Abcg2*$^{(-/-)}$ mice, but was unchanged between scans in *Abcb1a/b*$^{(-/-)}$*Abcg2*$^{(-/-)}$ mice (Table 3 and Figure 5). Furthermore, in baseline scans k_3 was significantly lower in *Abcb1a/b*$^{(-/-)}$*Abcg2*$^{(-/-)}$ mice as compared to wild-type, *Abcb1a/b*$^{(-/-)}$ and *Abcg2*$^{(-/-)}$ mice. $CL_{H,uptake}$ was in a similar range as the mouse liver blood flow rate (90 mL/min/kg)[28] and did not significantly change between scans in any of the studied mouse strains (Table 3). $CL_{H,bile}$ significantly decreased in scan 2 in all genotypes, except for *Abcb1a/b*$^{(-/-)}$*Abcg2*$^{(-/-)}$ mice. The kidney TACs appeared to be similar in scan 1 and scan 2 and between different genotypes (see Supporting Information, Figure S5). $CL_{R,uptake}$ did not show significant changes between scans, except for *Abcb1a/b*$^{(-/-)}$ mice, in which $CL_{R,uptake}$ was significantly decreased after tariquidar administration (see Supporting Information, Table S3).

In order to identify potential basolateral hepatocyte transporters for the uptake of [^{11}C]tariquidar from blood into the liver, we performed *in vitro* uptake experiments in transporter-overexpressing cells. No significant differences in tariquidar uptake were found between SLCO1B1-, 1B3-, and 2B1-overexpressing and vector control cells (Figure 6a). Furthermore, the uptake of tariquidar was not significantly different between wild-type cells and cells overexpressing SLC22A1, SLC22A2, SLC22A3 or SLC22A5, but significantly increased in cells overexpressing SLC22A4 (Figure 6b).

Discussion

We performed PET imaging with the dual ABCB1/ABCG2 substrate [^{11}C]tariquidar in humans and mice to assess whether the activities of hepatic canalicular ABCB1 and ABCG2 can be measured with this radiotracer. We found a marked decrease in the amount of radioactivity excreted into bile in both humans and mice when a pharmacological dose of unlabeled tariquidar was co-administered with the radiotracer, which suggested inhibition of canalicular efflux transport activity. Moreover, PET data in transporter knockout mice suggested that both ABCB1 and ABCG2 mediated biliary excretion of [^{11}C]tariquidar. Our findings are of relevance, as they extend previous PET imaging work of hepatic transporters to an assessment of canalicular efflux transporter activity and highlight the utility of pharmacokinetic modeling in measuring hepatic transport activity.

Our PET data were modeled using a previously described 3-compartment pharmacokinetic model (see Supporting Information, Figure S1).[27] The disposition of [^{11}C]tariquidar in the blood compartment was not modeled, but the time course of [^{11}C]tariquidar in blood was used as an input function to the model as is typically done for kinetic modeling of PET data. Since the liver receives dual blood supply *via* the hepatic artery (~25%) and the portal vein (~75%), the employed model considered a mathematically estimated, flow-weighted dual input function.[27] However, our approach to mathematically estimate the portal vein input function will require future validation, e.g. by comparison with an image-derived portal vein input function.

According to the investigator's brochure,[23] upon i.v. tariquidar administration in several species (rats, monkeys and humans) the drug is mainly excreted in the form of metabolites into feces with negligible urinary excretion. In none of the studied species circulating metabolites of tariquidar could be detected in plasma,[23] indicating that metabolites cannot distribute from liver back into blood or that they are rapidly eliminated from the liver. In the present study, metabolite analysis

confirmed in both, humans and mice, only a very low amount of radiolabeled metabolites in plasma during the time course of the PET scan. Moreover, in mouse liver and bile, only a small amount of radiolabeled metabolites of [^{11}C]tariquidar (< 13%) could be detected at 30 minutes after radiotracer injection (Table 2). Thus, it was assumed that metabolism in the liver was still negligible over the short duration of the PET scan, and therefore, our pharmacokinetic model represented the exchange of unmetabolized radiotracer between the different compartments.

In humans, k_1 showed a moderate but significant reduction, when unlabeled tariquidar was co-infused in scan 2 (Figure 3). Although this reduction in k_1 may indicate a partial inhibition of basolateral hepatic transporter(s) mediating the uptake of [^{11}C]tariquidar from blood into the liver, *in vitro* experiments proved that major human basolateral hepatic uptake transporters (SLCO1B1, SLCO1B3, SLCO2B1, SLC22A1 and SLC22A3) did not transport tariquidar (Figure 6). On the other hand, SLC22A4-overexpressing cells showed higher tariquidar uptake as compared to wild-type cells suggesting that tariquidar is a substrate of SLC22A4. However, while this transporter has been shown to be highly expressed in kidney, spleen, heart or fetal liver, expression in the adult liver is controversial.[31, 33, 36] Thus, there is at present no firm evidence for the involvement of basolateral hepatic uptake transporters in the distribution of tariquidar from blood into hepatocytes. Therefore, the moderate reduction in k_1 observed in scan 2 may be related to other reasons than inhibition of uptake transporters, such as changes in hepatic blood flow caused by administration of unlabeled tariquidar, assuming that k_1 is most likely blood flow dependent.

The co-administration of unlabeled tariquidar caused a reduction in the radioactivity excreted into bile, as reflected by a significant decrease in the k_3 parameter (Figures 3 and 5). PET data in *Abcb1a/b*$^{(-/-)}$*Abcg2*$^{(-/-)}$ mice, which showed a 2-fold lower k_3 value than wild-type mice (Figure 5), indicated that both ABCB1 and ABCG2 were involved in the biliary excretion of [^{11}C]tariquidar.

However, when only ABCB1A/B or ABCG2 were missing (*Abcb1a/b*$^{(-/-)}$ mice or *Abcg2*$^{(-/-)}$ mice) no reduction in k_3 was observed (Figure 5). A possible explanation for this could be a compensatory upregulation of hepatic ABCB1A/B in *Abcg2*$^{(-/-)}$ mice and of ABCG2 in *Abcb1a/b*$^{(-/-)}$ mice. This is supported by literature data, reporting approximately 2-fold increased ABCB1A protein expression in the liver of the same *Abcg2*$^{(-/-)}$ mouse strain as used in the present study relative to wild-type mice.[37] Our data thus suggest inhibition of hepatic ABCB1 and ABCG2 transport activity by unlabeled tariquidar leading to decreased biliary excretion of [^{11}C]tariquidar. The half maximum-inhibitory concentration (IC_{50}) of tariquidar to inhibit its own transport was found to be considerably lower for ABCB1 (17.1 nmol/L) than for ABCG2 (310.4 nmol/L),[19] which is in agreement with tariquidar being a more potent inhibitor of ABCB1 than of ABCG2. Accordingly, tariquidar could only inhibit ABCB1 and not ABCG2 activity at the human BBB when administered using the same i.v. infusion protocol as in the present study.[19] However, while unbound plasma concentrations of tariquidar may not be sufficiently high to inhibit ABCG2 at the human BBB, considerably higher concentrations may be achieved in liver tissue, resulting in a higher exposure of hepatic ABCG2 to tariquidar. AUC_{liver}/AUC_{blood} of [^{11}C]tariquidar was approximately 40 in the second PET scan in humans (see Supporting Information, Table S2), which indicates that total liver concentrations of tariquidar were higher (approximately 120 μmol/L) than the corresponding plasma concentrations. However, a relation of the unbound liver concentration of tariquidar to its *in vitro* IC_{50} for ABCG2 inhibition is not feasible as the extent of protein binding of tariquidar in the liver is not known.

Interestingly, data in carriers of the *ABCG2* SNP c.421C>A, which was shown to be associated with reduced ABCG2 protein abundance in the human liver,[38] pointed to reduced biliary excretion of [^{11}C]tariquidar as compared with non SNP carriers (Figure 3). However, this

preliminary finding needs to be confirmed in future studies with a larger sample size of subjects with different c.421C>A genotypes.

The impaired biliary excretion of [^{11}C]tariquidar was reflected by a significant increase in AUC_{blood} from scan 1 to scan 2 (see Supporting Information, Table S2). This scenario may be related to a scenario of the extended clearance model described by Patilea-Vrana,[3] in which, when a drug's passive permeability across the sinusoidal membrane is high, the inhibition of canalicular efflux clearance results in an increase in both systemic and liver concentrations of the drug. This scenario differs from the one described with other PET tracers (e.g. [^{11}C]dehydropravastatin and [^{11}C]rosuvastatin),[10, 12] for which sinusoidal uptake clearance is a major determinant of hepatic clearance.[3] In the present study, increased accumulation of radioactivity in the liver was not observed when biliary excretion was impaired and only a moderate increase was observed in the blood concentrations. The rise in liver radioactivity exposure due to impaired biliary excretion can be expected to be relatively small as biliary excretion occurred very slowly, as reflected by the very low rate constant k_3 (0.0009 ± 0.0007 min^{-1}) and the relatively low amount of radioactivity measured in excreted bile at the end of the first PET scan (0.8 ± 0.9% of the injected dose). It can be hypothesized that any rise in liver radioactivity exposure was masked by the reduction of k_1 in scan 2, which was caused by an unknown mechanism (e.g. a tariquidar-induced decrease in hepatic blood flow). An additional explanation for the lack of pronounced changes in blood pharmacokinetics may be the existence of an alternative excretion pathway. Previous data in healthy human volunteers and the present data in mice suggest that urinary excretion of radioactivity following i.v. injection of [^{11}C]tariquidar is very low. In healthy volunteers, approximately 2% of the injected dose was recovered from urine at the end of a 90-minute PET scan,[22] while in wild-type mice this amount was approximately 0.2%. According to the investigator's brochure, tariquidar may undergo direct

secretion from blood into the intestine through the gastrointestinal tract mucosa.[23] This may represent an alternative excretion pathway of tariquidar, which may come into play when biliary excretion is impaired. This is also supported by whole body distribution data of [^{11}C]tariquidar in healthy human volunteers, who showed moderate intestinal radioactivity uptake.[22] Our employed PET analysis was not capable of quantifying intestinal secretion of radioactivity, as the intestine was not within the field of view of the PET scanner in humans. In mice, on the other hand, the radioactivity signal in the intestine could be measured as the entire animal was within the field of view of the PET scanner, but we were not able to distinguish intestinal radioactivity arising from biliary excretion from intestinal radioactivity arising from direct secretion from blood.

In conclusion, our data suggest that [^{11}C]tariquidar can be used as a PET probe substrate to quantify ABCB1/ABCG2 transport activity in the liver. An advantage of [^{11}C]tariquidar over other previously reported PET tracers is its presumably good metabolic stability and the apparent lack of an involvement of hepatic uptake transporters, suggesting that canalicular efflux transporter activity can be measured without a possible confounding effect of uptake transporters. [^{11}C]Tariquidar may find use to assess the effect of DDIs, genetic polymorphisms and disease on hepatic transporter activity. Moreover, our data indicate that tariquidar in pharmacological doses can inhibit hepatic ABCB1 and ABCG2 transport activity, which may decrease hepatobiliary excretion of other ABCB1 and/or ABCG2 substrate drugs and qualify tariquidar as a prototypical hepatic ABCB1/ABCG2 inhibitor for DDI studies.

Acknowledgements

This work was supported by the Austrian Science Fund (FWF) [grant KLI 480-B30, to O. Langer] and by the Lower Austria Corporation for Research and Education (NFB) [grant LS15-003, to O. Langer]. B. Stieger is supported by the Swiss National Science Foundation [grant 310030_166563]. The authors wish to thank all members of the Preclinical Molecular Imaging group at AIT for support in preclinical PET imaging, Johann Stanek (Department of Clinical Pharmacology, Medical University of Vienna) for metabolite analysis in clinical PET imaging, Harald Ibeschitz (Division of Nuclear Medicine, Medical University of Vienna) for technical support in clinical PET imaging, Peter Marhofer and his team (Department of Anesthesia and Intensive Care Medicine, Medical University of Vienna) for arterial cannulation of study participants and Helmuth Haslacher (Department of Laboratory Medicine, Medical University of Vienna) for subject genotyping. Moreover, Rudolf Karch and Akihiro Matsuda are acknowledged for useful discussions and help with the development of the pharmacokinetic model and Csilla Özvegy-Laczka and Gergely Szakács (Hungarian Academy of Sciences, Budapest, Hungary) for providing the SLCO transporter-overexpressing cell lines.

Supporting Information

Pharmacokinetic model to describe the hepatobiliary distribution of [^{11}C]tariquidar. Tariquidar plasma concentrations during scan 2 and correlation with % change in k_3. Model fits in one representative subject. TACs in the human kidney cortex. TACs in arterial blood, liver, intestine and kidney for wild-type and transporter knockout mice. Model fits for mouse data. Table with demographic data and blood analysis results. Table with AUC values in different organs for

human and mouse data. Table with renal uptake clearance values for humans and mice. This material is available free of charge *via* the Internet at http://pubs.acs.org.

References

1. Shitara, Y.; Horie, T.; Sugiyama, Y. Transporters as a determinant of drug clearance and tissue distribution. *Eur. J. Pharm. Sci.* **2006**, *27*, (5), 425-46.
2. Patel, M.; Taskar, K. S.; Zamek-Gliszczynski, M. J. Importance of hepatic transporters in clinical disposition of drugs and their metabolites. *J. Clin. Pharmacol.* **2016**, *56 Suppl 7*, S23-39.
3. Patilea-Vrana, G.; Unadkat, J. D. Transport vs. metabolism: what determines the pharmacokinetics and pharmacodynamics of drugs? Insights from the extended clearance model. *Clin. Pharmacol. Ther.* **2016**, *100*, (5), 413-418.
4. Yee, S. W.; Brackman, D. J.; Ennis, E. A.; Sugiyama, Y.; Kamdem, L. K.; Blanchard, R.; Galetin, A.; Zhang, L.; Giacomini, K. M. Influence of transporter polymorphisms on drug disposition and response: a perspective from the international transporter consortium. *Clin. Pharmacol. Ther.* **2018**, *104*, (5), 803-817.
5. Gessner, A.; Konig, J.; Fromm, M. F. Clinical aspects of transporter-mediated drug-drug interactions. *Clin. Pharmacol. Ther.* **2019**, *105*, (6), 1386-1394.
6. Evers, R.; Piquette-Miller, M.; Polli, J. W.; Russel, F. G. M.; Sprowl, J. A.; Tohyama, K.; Ware, J. A.; de Wildt, S. N.; Xie, W.; Brouwer, K. L. R.; International Transporter, C. Disease-associated changes in drug transporters may impact the pharmacokinetics and/or toxicity of drugs: a white paper from the international transporter consortium. *Clin. Pharmacol. Ther.* **2018**, *104*, (5), 900-915.
7. Kusuhara, H. Imaging in the study of membrane transporters. *Clin. Pharmacol. Ther.* **2013**, *94*, (1), 33-6.
8. Testa, A.; Zanda, M.; Elmore, C. S.; Sharma, P. PET tracers to study clinically relevant hepatic transporters. *Mol. Pharm.* **2015**, *12*, (7), 2203-16.

9. Tournier, N.; Stieger, B.; Langer, O. Imaging techniques to study drug transporter function in vivo. *Pharmacol. Ther.* **2018**, *189*, 104-122.

10. Kaneko, K.; Tanaka, M.; Ishii, A.; Katayama, Y.; Nakaoka, T.; Irie, S.; Kawahata, H.; Yamanaga, T.; Wada, Y.; Miyake, T.; Toshimoto, K.; Maeda, K.; Cui, Y.; Enomoto, M.; Kawamura, E.; Kawada, N.; Kawabe, J.; Shiomi, S.; Kusuhara, H.; Sugiyama, Y.; Watanabe, Y. A clinical quantitative evaluation of hepatobiliary transport of [^{11}C]dehydropravastatin in humans using positron emission tomography. *Drug Metab. Dispos.* **2018**, *46*, (5), 719-728.

11. He, J.; Yu, Y.; Prasad, B.; Link, J.; Miyaoka, R. S.; Chen, X.; Unadkat, J. D. PET imaging of Oatp-mediated hepatobiliary transport of [^{11}C]rosuvastatin in the rat. *Mol. Pharm.* **2014**, *11*, (8), 2745-54.

12. Billington, S.; Shoner, S.; Lee, S.; Clark-Snustad, K.; Pennington, M.; Lewis, D.; Muzi, M.; Rene, S.; Lee, J.; Nguyen, T. B.; Kumar, V.; Ishida, K.; Chen, L.; Chu, X.; Lai, Y.; Salphati, L.; Hop, C.; Xiao, G.; Liao, M.; Unadkat, J. D. PET imaging of [^{11}C]rosuvastatin hepatic concentrations and hepatobiliary transport in humans in the absence and presence of cyclosporine A. *Clin. Pharmacol. Ther.* **2019**, *106*, (5), 1056-1066.

13. Sundelin, E. I.; Gormsen, L. C.; Jensen, J. B.; Vendelbo, M. H.; Jakobsen, S.; Munk, O. L.; Christensen, M. M.; Brosen, K.; Frokiaer, J.; Jessen, N. Genetic polymorphisms in organic cation transporter 1 attenuates hepatic metformin exposure in humans. *Clin. Pharmacol. Ther.* **2017**, *102*, (5), 841-848.

14. Takashima, T.; Kitamura, S.; Wada, Y.; Tanaka, M.; Shigihara, Y.; Ishii, H.; Ijuin, R.; Shiomi, S.; Nakae, T.; Watanabe, Y.; Cui, Y.; Doi, H.; Suzuki, M.; Maeda, K.; Kusuhara, H.; Sugiyama, Y. PET imaging-based evaluation of hepatobiliary transport in humans with (15*R*)-^{11}C-TIC-Me. *J. Nucl. Med.* **2012**, *53*, (5), 741-8.

15. Orntoft, N. W.; Munk, O. L.; Frisch, K.; Ott, P.; Keiding, S.; Sorensen, M. Hepatobiliary transport kinetics of the conjugated bile acid tracer ^{11}C-CSar quantified in healthy humans and patients by positron emission tomography *J. Hepatol.* **2017**, *67*, 321-327.

16. Bauer, M.; Matsuda, A.; Wulkersdorfer, B.; Philippe, C.; Traxl, A.; Özvegy-Laczka, C.; Stanek, J.; Nics, L.; Klebermass, E. M.; Poschner, S.; Jäger, W.; Patik, I.; Bakos, É.; Szakács, G.; Wadsak, W.; Hacker, M.; Zeitlinger, M.; Langer, O. Influence of OATPs on hepatic disposition of erlotinib measured with positron emission tomography *Clin. Pharmacol. Ther.* **2018**, *104*, (1), 139-147.

17. Bauer, M.; Traxl, A.; Matsuda, A.; Karch, R.; Philippe, C.; Nics, L.; Klebermass, E. M.; Wulkersdorfer, B.; Weber, M.; Poschner, S.; Tournier, N.; Jäger, W.; Wadsak, W.; Hacker, M.; Wanek, T.; Zeitlinger, M.; Langer, O. Effect of rifampicin on the distribution of [^{11}C]erlotinib to the liver, a translational PET study in humans and in mice. *Mol Pharm* **2018**, *15*, (10), 4589-4598.

18. Fox, E.; Bates, S. E. Tariquidar (XR9576): a P-glycoprotein drug efflux pump inhibitor. *Expert Rev. Anticancer Ther.* **2007**, *7*, (4), 447-59.

19. Bauer, M.; Römermann, K.; Karch, R.; Wulkersdorfer, B.; Stanek, J.; Philippe, C.; Maier-Salamon, A.; Haslacher, H.; Jungbauer, C.; Wadsak, W.; Jäger, W.; Löscher, W.; Hacker, M.; Zeitlinger, M.; Langer, O. Pilot PET study to assess the functional interplay between ABCB1 and ABCG2 at the human blood-brain barrier. *Clin. Pharmacol. Ther.* **2016**, *100*, (2), 131-141

20. Bankstahl, J. P.; Bankstahl, M.; Römermann, K.; Wanek, T.; Stanek, J.; Windhorst, A. D.; Fedrowitz, M.; Erker, T.; Müller, M.; Löscher, W.; Langer, O.; Kuntner, C. Tariquidar and elacridar are dose-dependently transported by p-glycoprotein and bcrp at the blood-brain

barrier: a small-animal positron emission tomography and in vitro study *Drug Metab. Dispos.* **2013**, *41*, (4), 754-762.

21. Bauer, M.; Karch, R.; Zeitlinger, M.; Stanek, J.; Philippe, C.; Wadsak, W.; Mitterhauser, M.; Jager, W.; Haslacher, H.; Müller, M.; Langer, O. Interaction of ^{11}C-tariquidar and ^{11}C-elacridar with P-glycoprotein and breast cancer resistance protein at the human blood-brain barrier. *J. Nucl. Med.* **2013**, *54*, (8), 1181-7.
22. Bauer, M.; Blaickner, M.; Philippe, C.; Wadsak, W.; Hacker, M.; Zeitlinger, M.; Langer, O. Whole-body distribution and radiation dosimetry of ^{11}C-elacridar and ^{11}C-tariquidar in humans. *J. Nucl. Med.* **2016**, *57*, (8), 1265-8.
23. Investigator Brochure (AZT-011) P-Glycoprotein Pump Inhibitor. Version Number: 14. Issue Date: June 24 2013. AzaTrius Pharmaceuticals Pvt Ltd, Mumbai, India.
24. Wanek, T.; Kuntner, C.; Bankstahl, J. P.; Mairinger, S.; Bankstahl, M.; Stanek, J.; Sauberer, M.; Filip, T.; Erker, T.; Müller, M.; Löscher, W.; Langer, O. A novel PET protocol for visualization of breast cancer resistance protein function at the blood-brain barrier. *J. Cereb. Blood Flow Metab.* **2012**, *32*, (11), 2002-2011.
25. Bauer, M.; Zeitlinger, M.; Todorut, D.; Böhmdorfer, M.; Müller, M.; Langer, O.; Jäger, W. Pharmacokinetics of single ascending doses of the p-glycoprotein inhibitor tariquidar in healthy subjects. *Pharmacology* **2013**, *91*, (1-2), 12-9.
26. Loening, A. M.; Gambhir, S. S. AMIDE: a free software tool for multimodality medical image analysis. *Mol. Imaging* **2003**, *2*, (3), 131-7.
27. Hernández Lozano, I.; Karch, R.; Bauer, M.; Blaickner, M.; Matsuda, A.; Wulkersdorfer, B.; Hacker, M.; Zeitlinger, M.; Langer, O. Towards improved pharmacokinetic models for the analysis of transporter-mediated hepatic disposition of drug molecules with positron emission tomography. *AAPS J.* **2019**, *21*, (4), 61.

28. Davies, B.; Morris, T. Physiological parameters in laboratory animals and humans. *Pharm. Res.* **1993**, *10*, (7), 1093-5.

29. Patik, I.; Szekely, V.; Nemet, O.; Szepesi, A.; Kucsma, N.; Varady, G.; Szakacs, G.; Bakos, E.; Ozvegy-Laczka, C. Identification of novel cell-impermeant fluorescent substrates for testing the function and drug interaction of Organic Anion-Transporting Polypeptides, OATP1B1/1B3 and 2B1. *Sci. Rep.* **2018**, *8*, (1), 2630.

30. Thevenod, F.; Ciarimboli, G.; Leistner, M.; Wolff, N. A.; Lee, W. K.; Schatz, I.; Keller, T.; Al-Monajjed, R.; Gorboulev, V.; Koepsell, H. Substrate- and cell contact-dependent inhibitor affinity of human organic cation transporter 2: studies with two classical organic cation substrates and the novel substrate cd2+. *Mol Pharm* **2013**, *10*, (8), 3045-56.

31. Tamai, I.; Yabuuchi, H.; Nezu, J.; Sai, Y.; Oku, A.; Shimane, M.; Tsuji, A. Cloning and characterization of a novel human pH-dependent organic cation transporter, OCTN1. *FEBS Lett.* **1997**, *419*, (1), 107-11.

32. Tamai, I.; China, K.; Sai, Y.; Kobayashi, D.; Nezu, J.; Kawahara, E.; Tsuji, A. Na(+)-coupled transport of L-carnitine via high-affinity carnitine transporter OCTN2 and its subcellular localization in kidney. *Biochim. Biophys. Acta* **2001**, *1512*, (2), 273-84.

33. Visentin, M.; van Rosmalen, B. V.; Hiller, C.; Bieze, M.; Hofstetter, L.; Verheij, J.; Kullak-Ublick, G. A.; Koepsell, H.; Phoa, S. S.; Tamai, I.; Bennink, R. J.; van Gulik, T. M.; Stieger, B. Impact of organic cation transporters (OCT-SLC22A) on differential diagnosis of intrahepatic lesions. *Drug Metab. Dispos.* **2017**, *45*, (2), 166-173.

34. Wlcek, K.; Koller, F.; Ferenci, P.; Stieger, B. Hepatocellular organic anion-transporting polypeptides (OATPs) and multidrug resistance-associated protein 2 (MRP2) are inhibited by silibinin. *Drug Metab. Dispos.* **2013**, *41*, (8), 1522-8.

35. Schroeder, A.; Eckhardt, U.; Stieger, B.; Tynes, R.; Schteingart, C. D.; Hofmann, A. F.; Meier, P. J.; Hagenbuch, B. Substrate specificity of the rat liver Na(+)-bile salt cotransporter in Xenopus laevis oocytes and in CHO cells. *Am. J. Physiol.* **1998**, *274*, (2 Pt 1), G370-5.

36. Koepsell, H. The SLC22 family with transporters of organic cations, anions and zwitterions. *Mol. Aspects Med.* **2013**, *34*, (2-3), 413-35.

37. Mennone, A.; Soroka, C. J.; Harry, K. M.; Boyer, J. L. Role of breast cancer resistance protein in the adaptive response to cholestasis. *Drug Metab. Dispos.* **2010**, *38*, (10), 1673-8.

38. Prasad, B.; Lai, Y.; Lin, Y.; Unadkat, J. D. Interindividual variability in the hepatic expression of the human breast cancer resistance protein (BCRP/ABCG2): Effect of age, sex, and genotype. *J. Pharm. Sci.* **2013**, *102*, (3), 787-93.

Figure Legends

Figure 1. Serial PET images of the abdominal region for baseline scan (scan 1) and scan with concurrent infusion of unlabeled tariquidar (scan 2) recorded at different time intervals after radiotracer injection. Radioactivity concentration is expressed as standardized uptake value (SUV). Anatomical structures are labeled with arrows (L: liver, GB: gall bladder).

Figure 2. Mean time-activity curves (SUV ± SD, n = 5, c.421AA subject for whom only scan 1 data are available is not included) for arterial blood (**a**), liver (**b**), and extrahepatic bile duct and gall bladder (eBD/GB, **c**) for baseline scan (scan 1) and scan with concurrent infusion of unlabeled tariquidar (scan 2).

Figure 3. Changes in outcome parameters between the first and second scans for [^{11}C]tariquidar hepatobiliary distribution in individual subjects. The rate constants for radioactivity transfer between blood and liver (k_1 and k_2, min^{-1}) are shown in (**a**) and (**b**). The rate constant defining the transfer of [^{11}C]tariquidar from liver to extrahepatic bile duct and gall bladder (k_3, min^{-1}) is shown in (**c**). Insert in (**c**) shows amplification of lower value data points. Different symbols are used according to c.421C>A genotype (c.421CC, n =4, black circles, c.421CA, n = 1, green triangle, c.421AA, n = 1, red diamond, only scan 1 data available). * $p < 0.05$, 2-sided paired t-test.

Figure 4. Serial PET images of wild-type mice for baseline scan (scan 1) and scan after pre-treatment with unlabeled tariquidar (scan 2) and for *Abcb1a/b*$^{(-/-)}$*Abcg2*$^{(-/-)}$ mice (baseline scan) recorded at different time intervals after radiotracer injection. Radioactivity concentration is

expressed as standardized uptake value (SUV). Anatomical structures are labeled with arrows (L: liver, GB: gall bladder, D: duodenum, I: intestine).

Figure 5. Outcome parameters for [^{11}C]tariquidar hepatobiliary distribution in different mouse genotypes for the baseline scan (scan 1) and scan after pre-treatment with unlabeled tariquidar (scan 2). In (**a**) and (**b**) the rate constants defining the transfer between blood and liver (k_1 and k_2, min^{-1}) are shown, while the rate constant for transfer from liver to excreted bile (k_3, min^{-1}) is shown in (**c**). * $p < 0.05$, ** $p < 0.01$, *** $p < 0.001$, **** $p < 0.0001$, one-way ANOVA followed by a Tukey's multiple-comparison test.

Figure 6. (a) Uptake (percent of applied dose per 10^6 cells, %AD/1×10^6 cells) of tariquidar at 0.3, 2, 5, 10, 15, 20 and 30 minutes incubation time in A431 cells transfected with empty vector (vector control, VC) or A431 cells overexpressing SLCO1B1, SLCO1B3 or SLCO2B1. (**b**) Uptake (pmol/mg protein) of tariquidar at 0 minutes and after 5 minutes incubation time in wild-type (WT) and SLC22A1-, SLC22A2-, SLC22A3-, SLC22A4- and SLC22A5-overexpressing HEK 293 cells. Results show the mean ± SD. Results are from 2-4 independent experiments with at least 3 technical replicates each. * $p < 0.05$, one-way ANOVA followed by a Tukey's multiple-comparison test against vector control or wild-type for each studied time point.

Table 1. Pharmacokinetic parameters for baseline scan and scan with concurrent infusion of unlabeled tariquidar in humans.

Parameter	Baseline scan	Tariquidar co-infusion	Percentage change
k_1 (min^{-1})	4.81 ± 0.94 (3-16)	4.01 ± 1.01 (3-7)*	-17± 13%
k_2 (min^{-1})	0.0022 ± 0.0028 (14-140)	0.0024 ± 0.0020 (13-130)	+18± 101%
k_3 (min^{-1})	0.0009 ± 0.0007 (1-3)	0.0002 ± 0.0002 (2-3)*	-74± 24%
$CL_{H,uptake}$ (mL/min/kg)	25.11 ± 5.41	20.64 ± 5.99*	-18± 13%
$CL_{H,bile}$ (mL/min/kg)	0.0187 ± 0.0149	0.0035 ± 0.0034	-74± 24%

Parameter estimates are given as mean ± SD (n = 5). Values in parentheses represent the range in percent coefficient of variation (%CV) of the parameters (parameter precision). Percentage change was calculated as the mean of the individual percentage changes from scan 1 to scan 2. * $p < 0.05$, two-tailed paired t-test for comparison with baseline scan. k_1 and k_2 are the rate constants for transfer of radioactivity between liver and blood, and k_3 is the rate constant describing transfer of radioactivity from liver to extrahepatic bile duct and gall bladder. $CL_{H,uptake}$ and $CL_{H,bile}$ are the hepatic uptake and biliary efflux clearances, calculated from k_1 and k_3, respectively: $CL_{H,uptake} = (k_1 \times V_{blood})/w_{body}$, and $CL_{H,bile} = (k_3 \times V_{liv})/w_{body}$, where V_{blood} (mL) is the volume of blood in the liver (0.25 mL of blood per mL of liver tissue), V_{liv} (mL) is the physiological volume of the liver and w_{body} is the subject's body weight.

Table 2. Percentage of unchanged [^{11}C]tariquidar in different tissues and fluids of female FVB wild-type mice measured at 30 minutes after radiotracer injection with radio-TLC.

Animal ID	% of unchanged [^{11}C]tariquidar					
	Plasma[a]	Plasma[a]	Liver	Bile	Kidneys	Urine
M150	84.2	78.6	93.3	90.2	96.4	19.9
M151	76.8	71.6	92.9	91.8	95.4	52.7
M152	92.5	70.9	92.6	80.5	93.6	37.7
M153	73.8	77.7	92.4	n.d.	94.2	42.1
Mean ± SD	*78.3 ± 6.7*		*92.8 ± 0.3*	*87.5 ± 5.0*	*94.9 ± 1.1*	*38.1 ± 11.8*

n.d.: not determined

[a] Two technical replicates for plasma

Table 3. Pharmacokinetic parameters for baseline scan and scan after pre-treatment with unlabeled tariquidar in mice.

Mice type	Parameter	Baseline scan	Tariquidar pre-treatment	Percentage change
Wild-type	k_1 (min^{-1})	8.92 ± 1.28 (2-3)	7.72 ± 0.98 (2-3)	-12 ± 14%
	k_2 (min^{-1})	0.13 ± 0.02 (2-4)	0.15 ± 0.04 (2-3)	+18 ± 23%
	k_3 (min^{-1})	0.0083 ± 0.0009 (1-2)	0.003 ± 0.001 (1-2)*	-62 ± 18%
	$CL_{H,uptake}$ (mL/min/kg)	145.20 ± 20.55	125.40 ± 15.88	-13 ± 14%
	$CL_{H,bile}$ (mL/min/kg)	0.54 ± 0.06	0.20 ± 0.08*	-62 ± 18%
Abcb1a/b$^{(-/-)}$ *Abcg2*$^{(-/-)}$	k_1 (min^{-1})	7.67 ± 2.32 (1-3)	8.18 ± 2.46 (2-3)	+10 ± 26%
	k_2 (min^{-1})	0.15 ± 0.05 (1-3)	0.19 ± 0.06 (2-3)	+29 ± 33%
	k_3 (min^{-1})	0.0038 ± 0.0005 (1-2)^{x}	0.0031 ± 0.0019 (1-11)	-14 ± 56%
	$CL_{H,uptake}$ (mL/min/kg)	124.70 ± 37.69	132.90 ± 39.88	+10 ± 26%
	$CL_{H,bile}$ (mL/min/kg)	0.24 ± 0.03^{xxx}	0.20 ± 0.13	-14 ± 56%
Abcb1a/b$^{(-/-)}$	k_1 (min^{-1})	7.86 ± 0.19 (2-4)	9.60 ± 2.49 (2-4)	+22 ± 32%
	k_2 (min^{-1})	0.12 ± 0.02 (2-4)	0.19 ± 0.06 (2-4)	+57 ± 55%
	k_3 (min^{-1})	0.0083 ± 0.0009 (1-2)	0.0030 ± 0.0012 (2-3)*	-62 ± 18%
	$CL_{H,uptake}$ (mL/min/kg)	127.7 ± 3.05	156.10 ± 40.37	+22 ± 32%
	$CL_{H,bile}$ (mL/min/kg)	0.54 ± 0.06	0.20 ± 0.08*	-62 ± 18%
Abcg2$^{(-/-)}$	k_1 (min^{-1})	7.17 ± 1.58 (2-6)	6.58 ± 2.24 (2-3)	-5 ± 37%
	k_2 (min^{-1})	0.15 ± 0.04 (2-5)	0.16 ± 0.07 (2-3)	+11 ± 51%
	k_3 (min^{-1})	0.008 ± 0.001 (1-2)	0.002 ± 0.001 (3-8)**	-77 ± 20%
	$CL_{H,uptake}$ (mL/min/kg)	116.5 ± 25.68	106.9 ± 36.31	-5 ± 37%
	$CL_{H,bile}$ (mL/min/kg)	0.49 ± 0.09	0.11 ± 0.09**	-77 ± 21%

Each value represents mean ± SD (n = 4-5 per group). Values in parentheses represent the range in percent coefficient of variation (%CV) of the parameters (parameter precision). Percentage change was calculated as the mean of the individual percentage changes from scan 1 to scan 2. * $p < 0.05$, ** $p < 0.01$, two-tailed paired t-test for comparison of second scan with baseline scan. ^{x} $p < 0.05$, ^{xxx} $p < 0.001$, one-way ANOVA followed by a Tukey's multiple-comparison test for comparison of parameters between wild-type mice and the three knockout strains. k_1 and k_2 are the rate constants for transfer of radioactivity between liver and blood, and k_3 is the rate constant

describing transfer of radioactivity from the liver to the excreted bile in the intestine. $CL_{H,uptake}$ and $CL_{H,bile}$ are the hepatic uptake and biliary efflux clearances, calculated from k_1 and k_3, respectively: $CL_{H,uptake} = (k_1 \times V_{blood})/w_{body}$, and $CL_{H,bile} = (k_3 \times V_{liv})/w_{body}$, where V_{blood} (mL) is the volume of blood in the liver (0.25 mL of blood per mL of liver tissue), V_{liv} (mL) is the physiological volume of the liver and w_{body} is the subject's body weight.

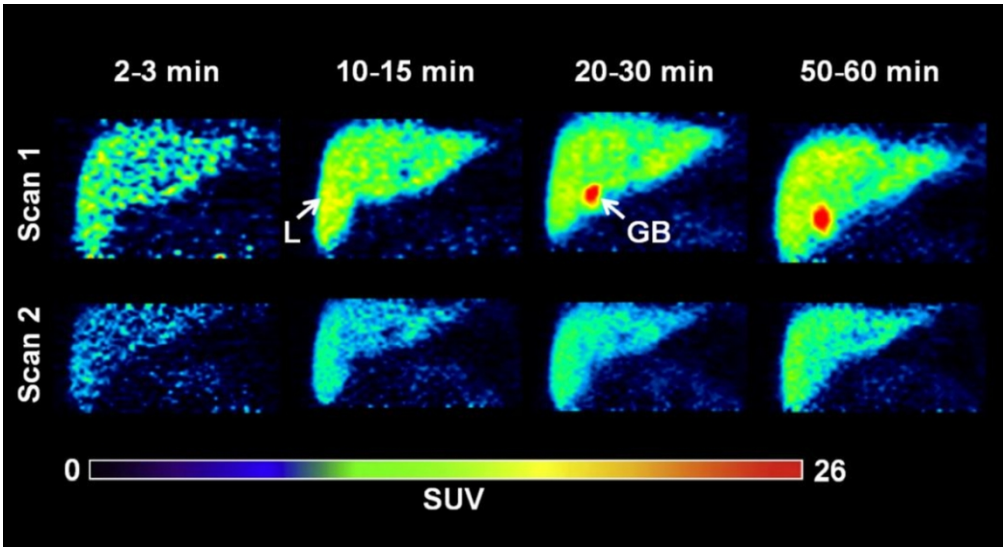

Figure 1

177x96mm (300 x 300 DPI)

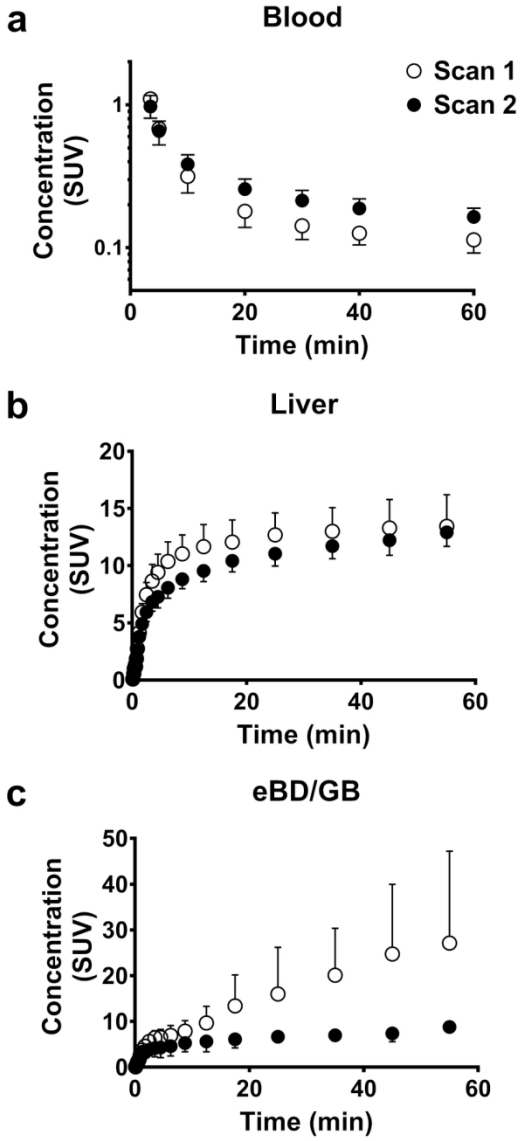

Figure 2

86x177mm (300 x 300 DPI)

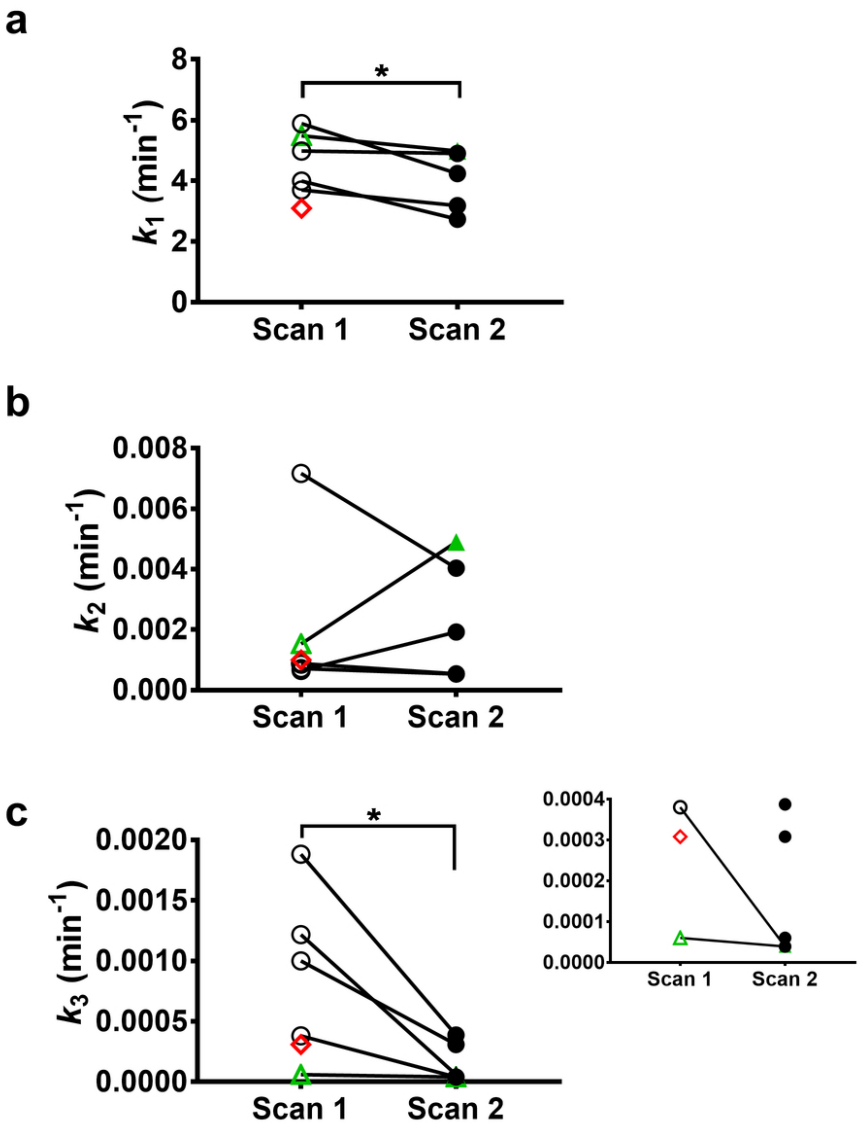

Figure 3

83x104mm (300 x 300 DPI)

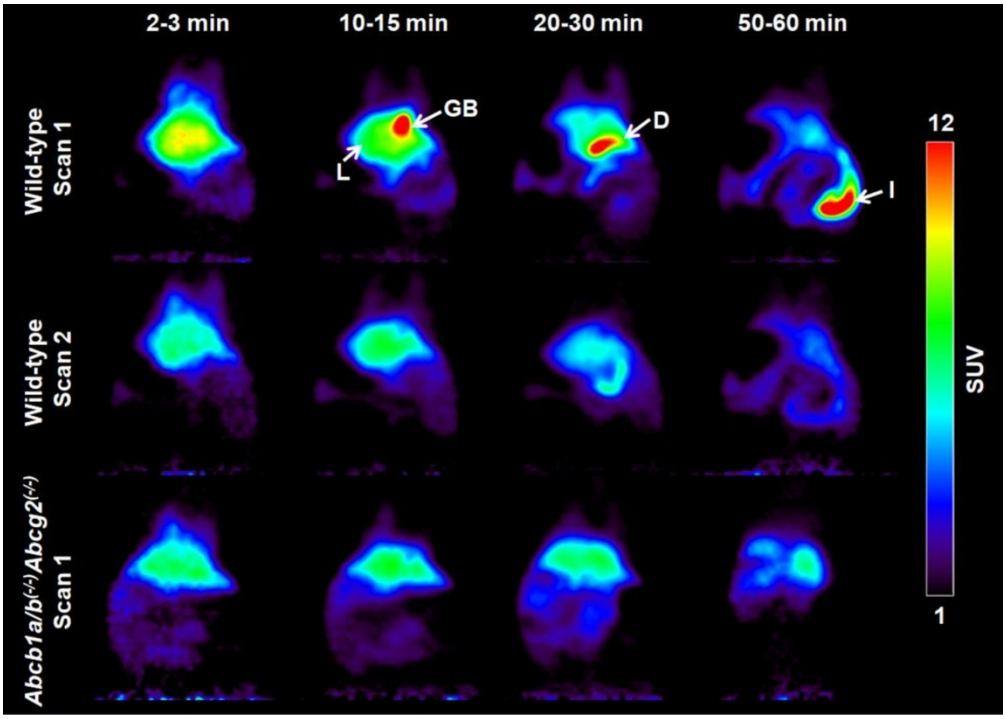

Figure 4

177x126mm (300 x 300 DPI)

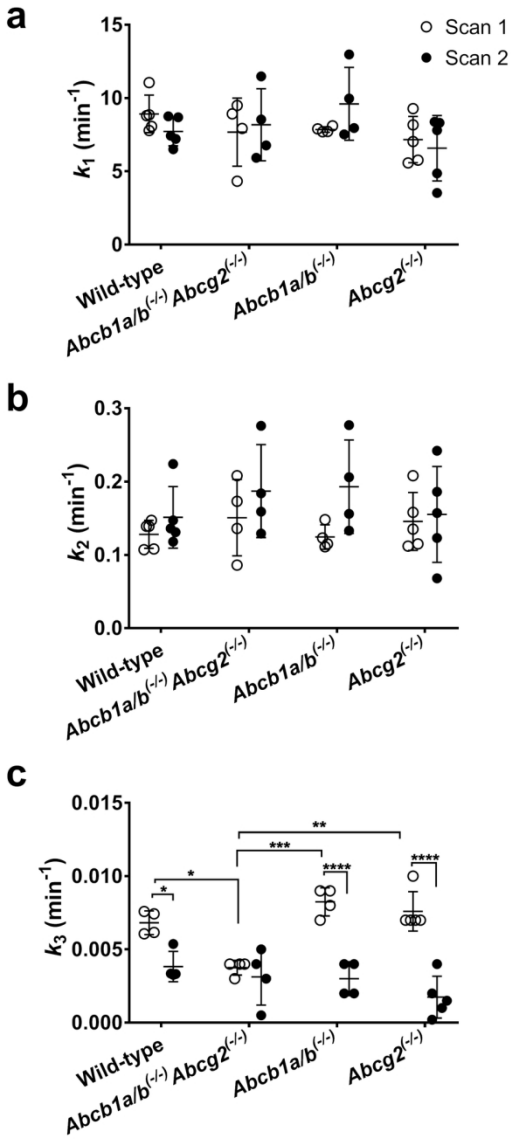

Figure 5

86x185mm (300 x 300 DPI)

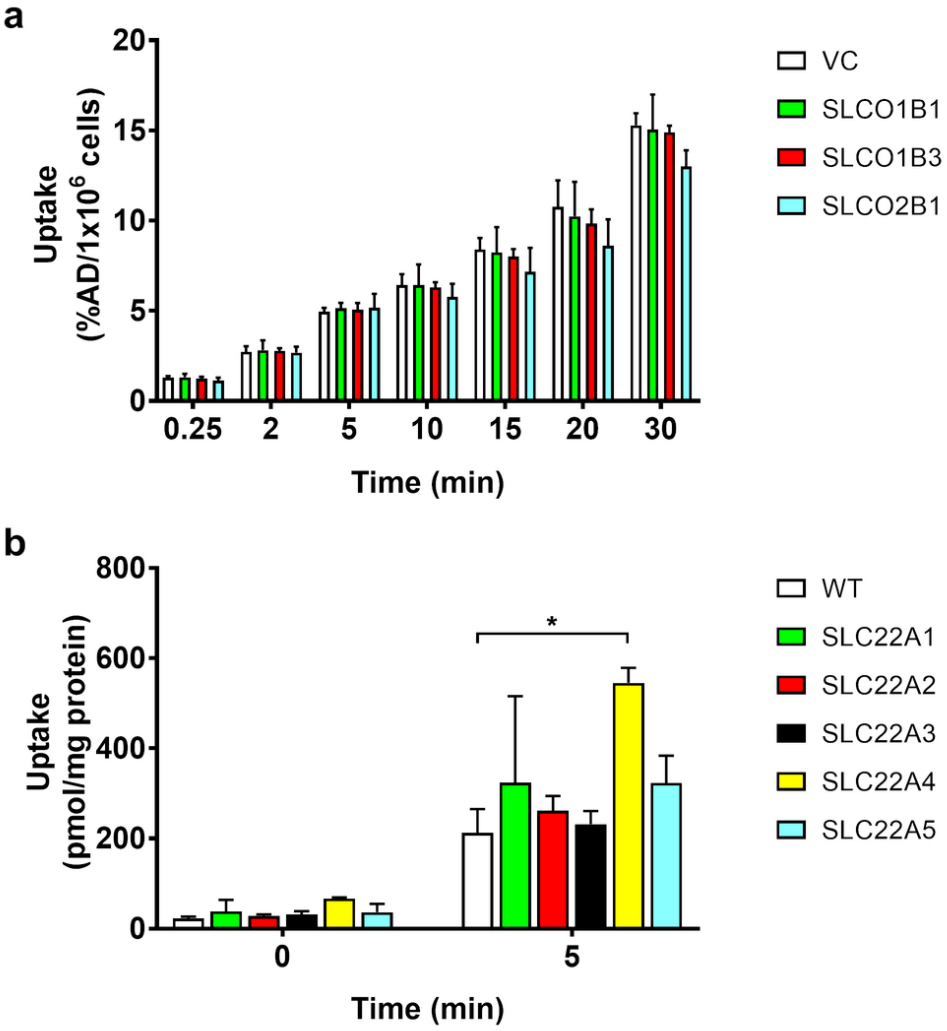

Figure 6

86x93mm (300 x 300 DPI)

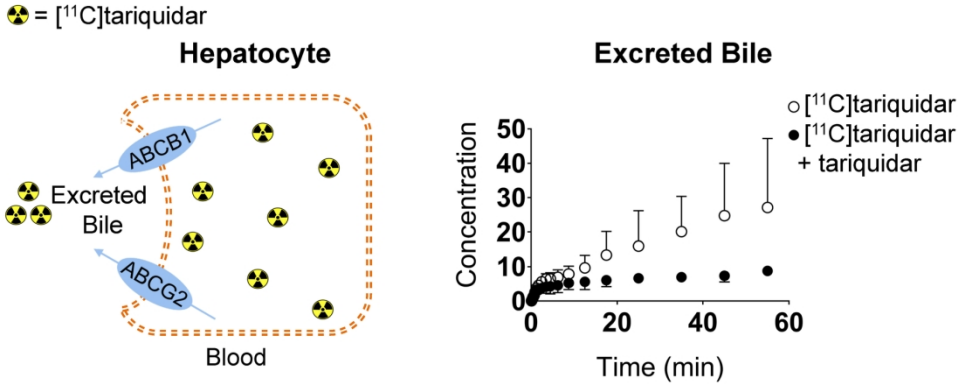

Graphical abstract

82x33mm (600 x 600 DPI)